Supporting Information

A strategy to unlock the potential of CrN as highly active oxygen reduction reaction catalyst

Junming Luo[a,b], Xiaochang Qiao[d], Jutao Jin[d], Xinlong Tian[e], Hongbo Fan[a,*], Demei Yu[b], Wenlong Wang[d], Shijun Liao[c,*] Neng Yu[f] and Yijie Deng[a,b]

[a] School of Environment and Civil Engineering, Dongguan University of Technology, Dongguan 523808, People's Republic of China

[b] School of Science, Xi'an Jiaotong University, Xi'an 710049, People's Republic of China

[c] The Key Laboratory of Fuel Cell Technology of Guangdong Province & The Key Laboratory of New Energy Technology of Guangdong Universities, School of Chemistry and Chemical Engineering, South China University of Technology, Guangzhou 510641, People's Republic of China

[d] School of Materials Science and Engineering, Dongguan University of Technology, Dongguan 523808, People's Republic of China

[e] State Key Laboratory of Marine Resource Utilization in South China Sea, Hainan University, Haikou 570228, People's Republic of China

[f] State Key Laboratory of Nuclear Resources and Environment, East China University of Technology, Nanchang 330013, People's Republic of China

* Corresponding author, e-mail address: fhb666666@126.com, chsjliao@scut.edu.cn

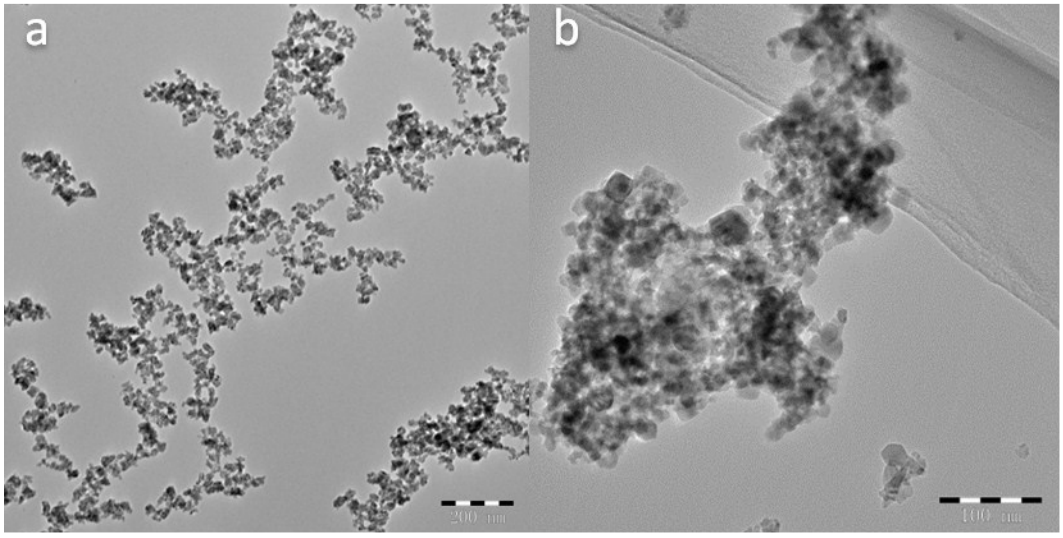

Figure S1. TEM images of free-standing CrN annealed at 750°Cin NH_3 atmosphere for 2 h.

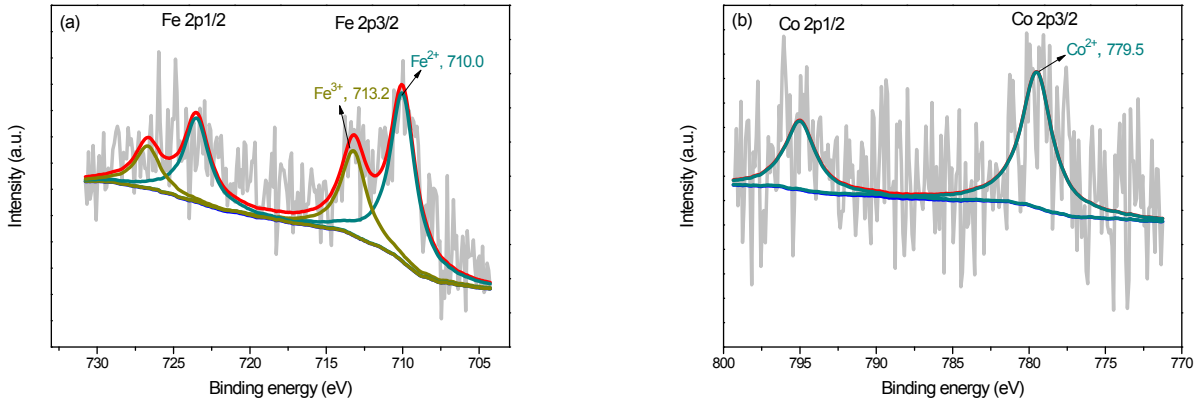

Figure S2. XPS spectra of (a) Fe 2p in $Cr_{10}Fe_2$/Z8C and (b) Co 2p in $Cr_{10}Co_2$/Z8C.

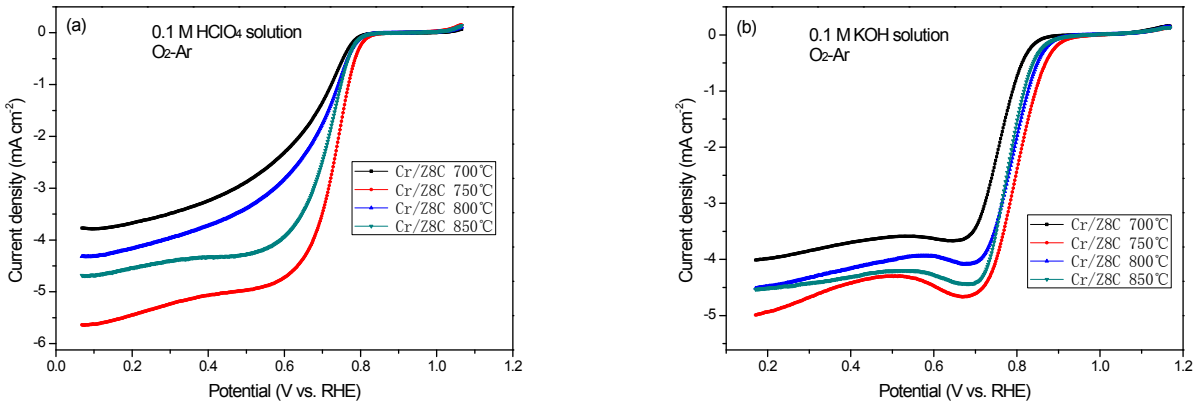

Figure S3. Linear sweep voltammetry curves of Cr/Z8C annealing at different temperatures (a) in 0.1 M $HClO_4$ solution and (b) 0.1 M KOH solution, calculated by substracting Ar-saturated solution from O_2-saturated solution at a rotation speed of 1600 rpm.

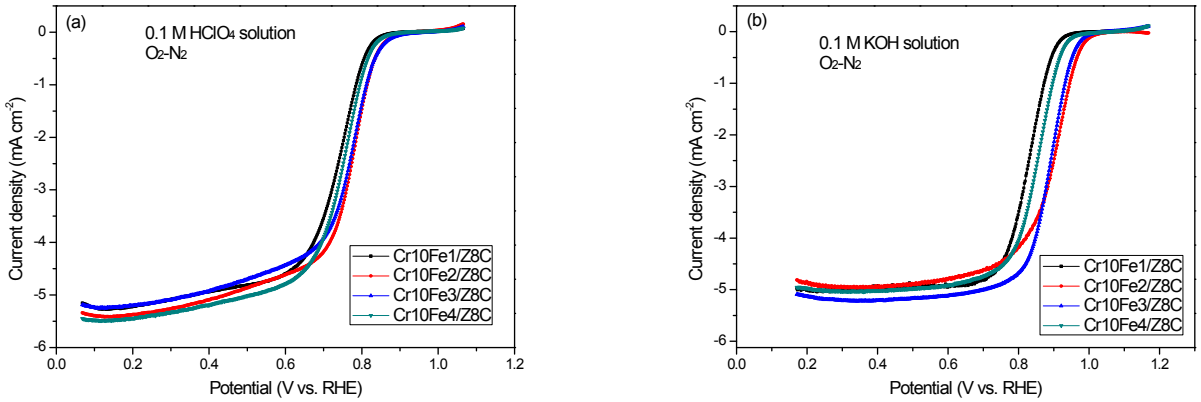

Figure S4. Linear sweep voltammetry curves of $Cr_{10}Fe_x$/Z8C annealing at 750℃ (a) in 0.1 M $HClO_4$ solution and (b) 0.1 M KOH solution, calculated by substracting Ar-saturated solution from O_2-saturated solution at a rotation speed of 1600 rpm.

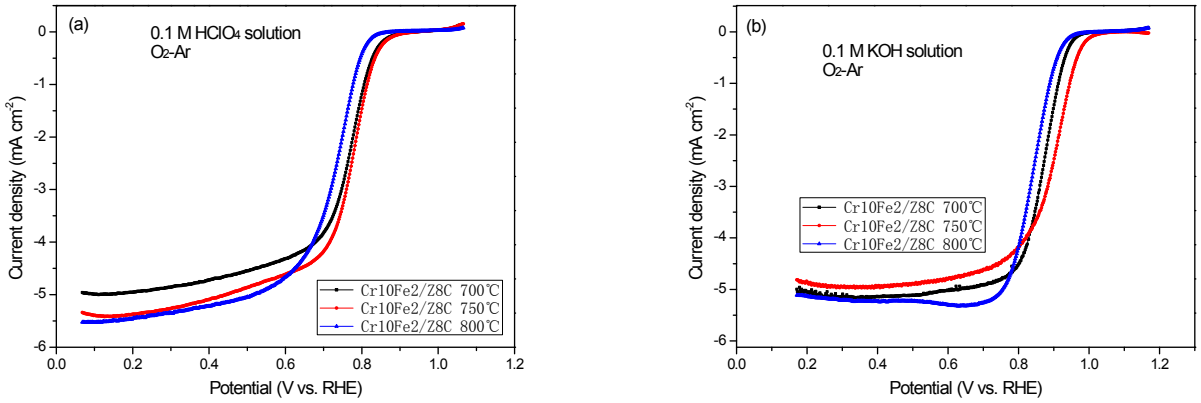

Figure S5. Linear sweep voltammetry curves of $Cr_{10}Fe_2$/Z8C annealing at different temperature (a) in 0.1 M $HClO_4$ solution and (b) 0.1 M KOH solution, calculated by substracting Ar-saturated solution from O_2-saturated solution at a rotation speed of 1600 rpm.

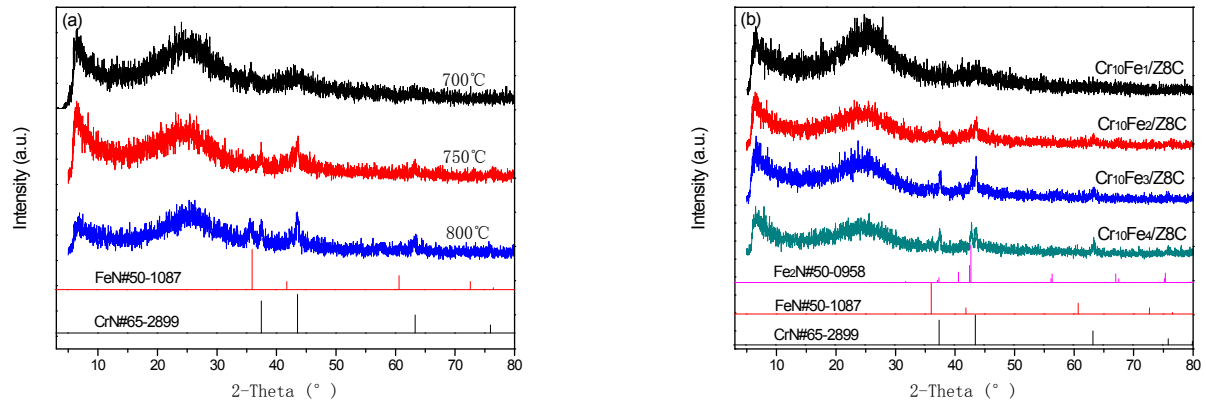

Figure S6. (a) XRD patterns of $Cr_{10}Fe_2$/Z8C annealed at different temperatures in an NH_3 atmosphere for 2 h; (b) XRD patterns of $Cr_{10}Fe_x$/Z8C (x= 1, 2, 3, 4) annealed at 750℃ in an NH_3 atmosphere for 2 h.

Figure S6a shows that clear diffraction peaks of CrN can only be found in the patterns of $Cr_{10}Fe_2$/Z8C

annealed at 750 and 800℃, while the FeN phase can be found in the patterns of $Cr_{10}Fe_2$/Z8C annealed at 700 and 800℃. This is probably because that Fe could be fully doped in the lattice of CrN at 750℃, as the annealing temperature rises, the doping capacity decreases therefore the FeN phase appeared again. As shown in Figure S6b, the Cr/Fe molar ratio higher than 10:2 resulted in the formation of FeN and Fe_2N, which is very likely that the amount of Fe surpassed the doping capacity therefore the excess Fe appeared as FeN and Fe_2N. In addition, it can be seen that the Cr/Fe molar ratio lower than 10:2 resulted in no clear diffraction peaks of CrN. This is probably that the amount of Fe was too low to destroy the structure of ZIF-8 to form detectable CrN crystals.

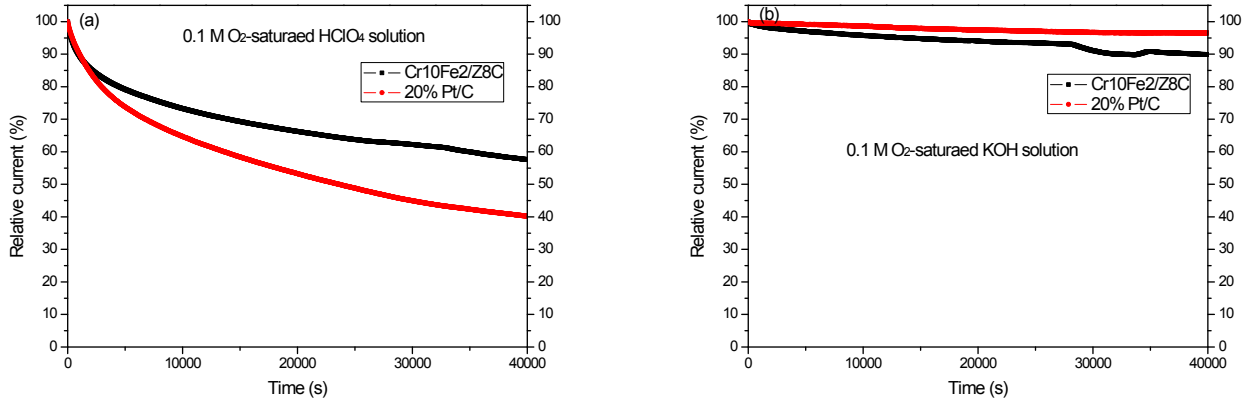

Figure S7. Catalytic stability of $Cr_{10}Fe_2$/Z8C and Pt/C polarized at 0.7 V vs. RHE during 40,000 s in (a) 0.1 M O_2-saturated $HClO_4$ solution and (b) 0.1 M O_2-saturated KOH solution.

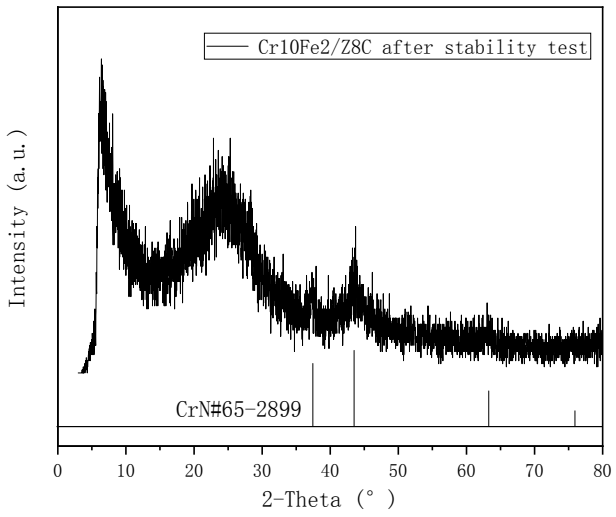

Figure S8. XRD pattern of $Cr_{10}Fe_2$/Z8C after stability tests.

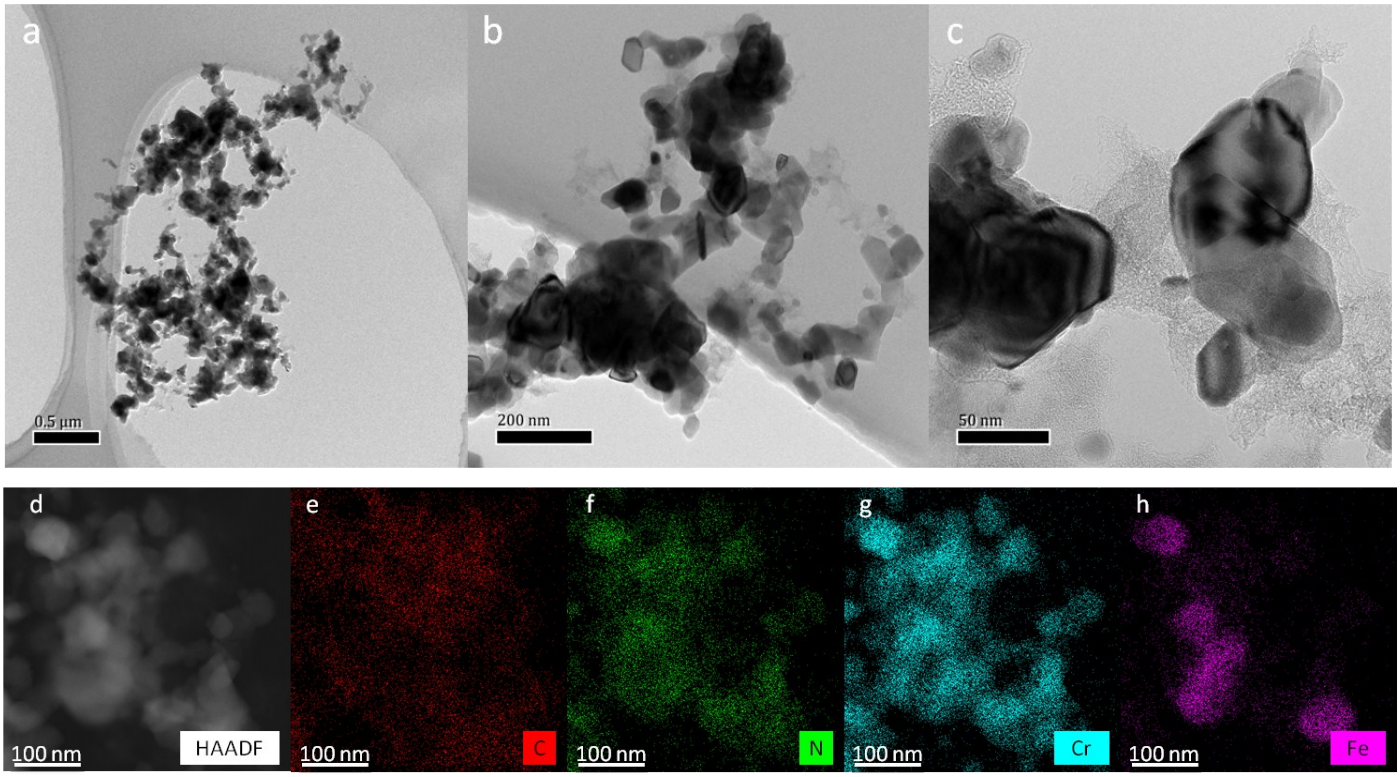

Figure S9. TEM images (a-c), HAADF images and EDS elemental mappings (d-h) of $Cr_{10}Fe_2$/Z8C after stability tests.

Table S1. Atomic contents of Cr/Z8C, $Cr_{10}Fe_2$/Z8C, $Cr_{10}Co_2$/Z8C in EDX analysis.

Sample	Atomic contents (%)						
	C	N	Cr	Fe	Co	Cr/Fe	Cr/Co
Cr/Z8C	86.71	12.74	0.55	-	-	-	-
$Cr_{10}Fe_2$/Z8C	97.33	2.39	0.16	0.1	-	1.6	-
$Cr_{10}Co_2$/Z8C	97.13	2.64	0.11	-	0.1	-	1.1

Table S2. Atomic contents of Cr/Z8C, $Cr_{10}Fe_2$/Z8C, $Cr_{10}Co_2$/Z8C and N-Z8C in XPS analysis.

Sample	Atomic contents (%)						
	C	N	O	Cr	Zn	Fe	Co
Cr/Z8C	79.24	10.23	8.37	1.37	0.78	-	-
$Cr_{10}Fe_2$/Z8C	89.24	4.99	5.04	0.41	0.15	0.16	-
$Cr_{10}Co_2$/Z8C	89.22	3.71	6.37	0.22	0.17	-	0.31
N-Z8C	88.14	7.67	3.36	-	0.83	-	-

Table S3. List of outstanding metal nitrides-based ORR catalysts in acidic and alkaline media.

Catalyst	Electrolyte	Half-wave potential (V vs. RHE)	Reference
$Ti_{0.8}Co_{0.2}N$ assemblies	0.1 M $HClO_4$	0.79	[1]
$Cr_{10}Fe_2$/Z8C	0.1 M $HClO_4$	0.768	This work
$Cr_{10}Co_2$/Z8C	0.1 M $HClO_4$	0.738	This work
Cr/Z8C	0.1 M $HClO_4$	0.722	This work
$Ti_{0.95}Ni_{0.05}N$	0.1 M $HClO_4$	0.70	[2]
$Co_{0.5}Mo_{0.5}N_y$/NCNCs	0.5 M H_2SO_4	0.58	[3]
TiON	0.5 M H_2SO_4	0.58	[4]
$Co_{0.6}Mo_{1.4}N_2$	0.1 M $HClO_4$	0.5	[5]
$Cr_{10}Fe_2$/Z8C	0.1 M KOH	0.901	This work
$Cr_{10}Co_2$/Z8C	0.1 M KOH	0.851	This work
$Ti_{0.8}Co_{0.2}N$ assemblies	0.1 M KOH	0.85	[1]
$Ti_{0.95}Ni_{0.05}N$	0.1 M KOH	0.80	[2]
$V_{0.95}Co_{0.05}N$ MFs	0.1 M KOH	0.80	[6]
Cr/Z8C	0.1 M KOH	0.797	This work
$V_{0.95}Co_{0.05}N$	0.1 M KOH	0.76	[7]
CoMoON	0.1 M KOH	0.76	[8]

References

[1] X.L. Tian, L. Wang, B. Chi, Y. Xu, S. Zaman, K. Qi, H. Liu, S. Liao, B.Y. Xia, Formation of a Tubular Assembly by Ultrathin Ti0.8Co0.2N Nanosheets as Efficient Oxygen Reduction Electrocatalysts for Hydrogen–/Metal–Air Fuel Cells, Acs Catal, (2018) 8970-8975.

[2] X.L. Tian, J.M. Luo, H.X. Nan, Z.Y. Fu, J.H. Zeng, S.J. Liao, Binary transition metal nitrides with enhanced activity and durability for the oxygen reduction reaction, J Mater Chem A, 3 (2015) 16801-16809.

[3] T. Sun, Q. Wu, R.C. Che, Y.F. Bu, Y.F. Jiang, Y. Li, L.J. Yang, X.Z. Wang, Z. Hu, Alloyed Co-Mo Nitride as High-Performance Electrocatalyst for Oxygen Reduction in Acidic Medium, Acs Catal, 5 (2015) 1857-1862.

[4] M. Chisaka, Y. Ando, N. Itagaki, Activity and durability of the oxygen reduction reaction in a nitrogen-doped rutile-shell on TiN-core nanocatalysts synthesised via solution-phase combustion, J Mater Chem A, 4 (2016) 2501-2508.

[5] B.F. Cao, J.C. Neuefeind, R.R. Adzic, P.G. Khalifah, Molybdenum Nitrides as Oxygen Reduction

Reaction Catalysts: Structural and Electrochemical Studies, Inorg Chem, 54 (2015) 2128-2136.

[6] H.B. Tang, J.M. Luo, X.L. Tian, Y.Y. Dong, J. Li, M.R. Liu, L.N. Liu, H.Y. Song, S.J. Liao, Template-Free Preparation of 3D Porous Co-Doped VN Nanosheet-Assembled Microflowers with Enhanced Oxygen Reduction Activity, Acs Appl Mater Inter, 10 (2018) 11604-11612.

[7] J.M. Luo, X.L. Tian, J.H. Zeng, Y.W. Li, H.Y. Song, S.J. Liao, Limitations and Improvement Strategies for Early-Transition-Metal Nitrides as Competitive Catalysts toward the Oxygen Reduction Reaction, Acs Catal, 6 (2016) 6165-6174.

[8] B.F. Cao, G.M. Veith, R.E. Diaz, J. Liu, E.A. Stach, R.R. Adzic, P.G. Khalifah, Cobalt Molybdenum Oxynitrides: Synthesis, Structural Characterization, and Catalytic Activity for the Oxygen Reduction Reaction, Angew Chem Int Edit, 52 (2013) 10753-10757.